



Measurement of the inclusive jet cross section  
in  $p\bar{p}$  collisions at  $\sqrt{s} = 1.96$  TeV

The DØ Collaboration  
URL: <http://www-d0.fnal.gov>

(Dated: January 13, 2008)

We report on a measurement of the inclusive jet cross section in  $p\bar{p}$  collisions at a center-of-mass energy  $\sqrt{s} = 1.96$  TeV which uses data collected by the DØ experiment at the Fermilab Tevatron Collider corresponding to an integrated luminosity of  $0.7 \text{ fb}^{-1}$ . Jets are reconstructed using the Run II midpoint cone jet algorithm. The data cover jet transverse momentum above 50 GeV, and jet rapidities up to 2.4. Detailed studies of correlations between systematic uncertainties in transverse momentum and rapidity are given, and results are found to be in good agreement with next-to-leading order QCD calculations. The data can be used to further constrain the parton distribution functions in the proton, especially the gluon density.

*Preliminary Results for Winter 2008 Conferences*

The cross section for the inclusive production of jets in hadron collisions provides stringent tests of Quantum Chromodynamics (QCD) over many orders of magnitude. When the transverse momentum ( $p_T$ ) of the jet with respect to the nominal beam axis is large, contributions from long-distance processes with low  $p_T$  are small and the production of jets can be calculated in perturbative QCD (pQCD). The inclusive jet cross section in  $p\bar{p}$  collisions at large  $p_T$  is directly sensitive to the strong coupling constant ( $\alpha_s$ ) and the parton distribution functions (PDFs) of the proton. Potential deviations from pQCD predictions at large  $p_T$  may indicate new physical phenomena not described by the Standard Model.

In this note, we report on a new measurement of the inclusive jet cross section in  $p\bar{p}$  collisions at a center-of-mass energy  $\sqrt{s} = 1.96$  TeV. The cross section is presented in six bins of jet rapidity ( $y$ ), extending out to  $|y| = 2.4$ , as a function of jet  $p_T$ . The data sample, collected with the D0 detector in 2004–2005 in Run II of the Fermilab Tevatron Collider, corresponds to an integrated luminosity of  $\mathcal{L} = 0.7 \text{ fb}^{-1}$  [1]. This measurement improves earlier inclusive jet cross section measurements by the CDF and D0 collaborations in Run I and Run II [2–4] and improves the present experimental precision on the inclusive jet cross section. The increased  $p\bar{p}$  center-of-mass energy between Run I and Run II ( $\sqrt{s} = 1.8$  to 1.96 TeV) leads to a significant increase in the cross section at large  $p_T$  — a factor three at  $p_T \sim 500$  GeV. Together with the increased luminosity in Run II, and the significantly reduced systematic uncertainties, this makes stringent tests of pQCD possible in a completely new kinematic domain. Special attention was given to sources of systematic errors and their correlations which will make it possible to further constrain the PDFs, especially the gluon density at high proton momentum fraction. These data are expected to have a strong impact on searches for new particles and extra dimensions, which suffer from poor knowledge of PDFs [5].

The primary tool for jet detection is the compensating, finely segmented, liquid-argon and uranium calorimeter that has almost complete solid angular coverage [6]. The central calorimeter (CC) covers the pseudorapidity [7] region  $|\eta| < 1.1$  and two endcap calorimeters (EC) extend the coverage up to  $|\eta| \sim 4.2$ . The intercryostat region (ICR) between the CC and EC contains scintillator-based detectors that supplement the coverage of the calorimeter. The Run II iterative seed-based cone jet algorithm including mid-points [8] with cone radius  $\mathcal{R} = \sqrt{(\Delta y)^2 + (\Delta\phi)^2} = 0.7$  in rapidity  $y$  and azimuthal angle  $\phi$  is used to cluster energies deposited in calorimeter towers. Jets are described in terms of their  $p_T$  and  $y$ . The binning in jet  $p_T$  is commensurate with the measured resolution. The same algorithm is used for partons in the pQCD calculations.

Events are required to satisfy jet trigger requirements. Only jets above a given transverse momentum threshold are kept by the highest level trigger (L3). The effective luminosity used in this analysis for the different triggers is 0.1, 1.5, 17, 73, 500, and 700  $\text{pb}^{-1}$  for the 15, 25, 45, 65, 95 and 125 GeV L3 trigger  $p_T$  thresholds, respectively. The jet  $p_T$  spectra from different triggers are combined together (starting from 98% efficiency) to form a continuous spectrum in  $p_T$ . The cross section is corrected for any jet trigger inefficiencies determined using muon-based triggers without any requirement on jet presence in the event.

The jet  $p_T$  is corrected for the energy response of the calorimeter, showering effects due to uninstrumented material, and energy deposits originating from event pile-up. The jet energy corrections bring the calorimeter jet 4-momentum to the particle level energy. The electromagnetic part of the calorimeter is calibrated using  $Z \rightarrow e^+e^-$  events [18]. The jet response for the jet pseudorapidity region [7]  $|\eta| < 0.4$  is determined using the momentum imbalance in  $\gamma$ +jet events. The  $p_T$  imbalance in dijet events with one jet in pseudorapidity [7]  $|\eta| < 0.4$  and the other anywhere in  $\eta$  is used to intercalibrate the jet response in  $\eta$ , as a function of jet  $p_T$ . Jet energy scale corrections are typically  $\approx 45\%$  of the jet energy at 50 GeV, and  $\approx 20\%$  at 400 GeV. Further corrections due to the difference in response between quark- and gluon-initiated jets are computed using the PYTHIA [9] Monte Carlo event generator, passed through a GEANT-based [10] simulation of the detector response in which the single-pion response was scaled to give the same jet response for data and simulation in  $\gamma$ +jet events. These corrections amount to  $\approx +4\%$  at jet energies of 50 GeV and  $\approx -2\%$  at 400 GeV in the CC. The relative uncertainty of the jet  $p_T$  calibration ranges from 1% at  $p_T \sim 100$  GeV to 1.5% at 500 GeV in the CC, and 1.5–2% in the ICR and EC.

The position of the  $p\bar{p}$  interaction is reconstructed using a tracking system consisting of silicon microstrip detectors and scintillating fibers located inside a solenoidal magnetic field of 2 T [6]. The position of the vertex along the nominal beamline is required to be within 50 cm of the detector center. The acceptance of this cut is  $93.0 \pm 0.5\%$ . A requirement is placed on the missing transverse energy ( $\cancel{E}_T$ ) in the event, computed as the transverse component of the vector sum of the momenta in the calorimeter cells, to suppress cosmic rays. The  $\cancel{E}_T$  is required to be  $< 0.7 p_T^{\text{max}}$  for  $p_T^{\text{max}} < 100$  GeV and  $< 0.5 p_T^{\text{max}}$  otherwise, where  $p_T^{\text{max}}$  is the maximum uncorrected jet  $p_T$  in the event. This requirement removes the cosmic ray background and is  $> 99.5\%$  efficient for signal. Cuts on characteristics of shower development for genuine jets are used to remove the remaining background due to electrons, photons and detector noise that mimic jets. The efficiency for these cuts is  $> 99\%$  ( $> 97.5\%$  in the ICR), determined using the tag-and-probe method in dijet events. In this method one good jet acts as the tag to ensure the event is good and another back-to-back jet acts as the probe that is used for measuring the efficiency. The D0 detector simulation [6] provides a good description of jet properties including characteristics of the shower development. Jet energy not contained in the calorimeter at very high energies ( $> 300$  GeV) worsens the  $p_T$  resolution and is included in the simulation.

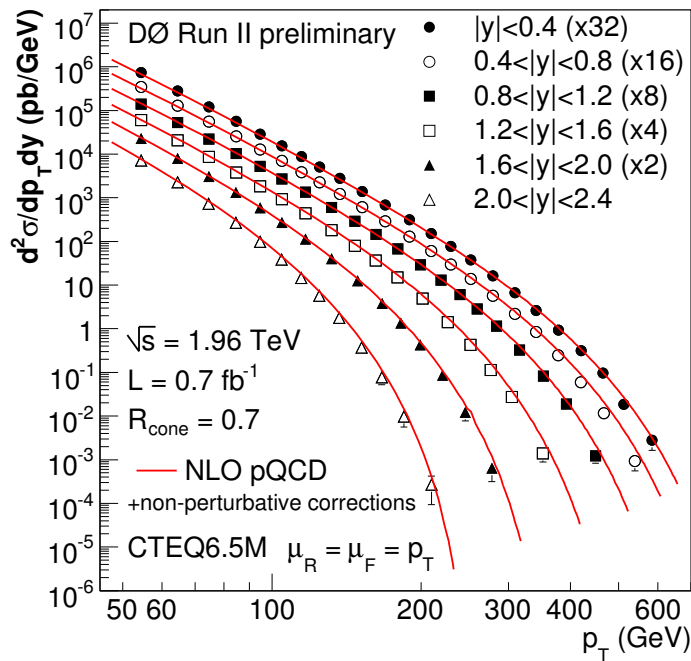


FIG. 1: The inclusive jet cross section as a function of jet  $p_T$  in six  $|y|$  bins. The data points are multiplied by 2, 4, 8, 16 and 32 for the bins  $1.6 < |y| < 2.0$ ,  $1.2 < |y| < 1.6$ ,  $0.8 < |y| < 1.2$ ,  $0.4 < |y| < 0.8$ , and  $|y| < 0.4$ , respectively. The errors are the statistical and systematic uncertainties (only larger of the two visible). Results from NLO pQCD calculations, with renormalization and factorization scales set to jet  $p_T$  using the CTEQ6.5M PDFs and including non-perturbative corrections, are compared to the data.

Systematic shifts in  $y$ , 0.01 in CC, 0.02 in EC, and 0.04 in ICR, due primarily to detector and jet algorithm effects, are also obtained using the simulation. The correction for muons and neutrinos, not reconstructed within jets, is determined using PYTHIA [9, 10] and is 2% independent of  $p_T$  and  $y$ .

The corrections for jet migration between bins in  $p_T$  and  $y$  due to finite resolution in position and energy are determined in an unfolding procedure, based on the experimental  $y$  and  $p_T$  resolutions. The jet  $p_T$  resolution is obtained using the  $p_T$  imbalance in dijet events and is found to decrease from 13% at  $p_T \sim 50$  GeV to 7% at  $p_T \sim 400$  GeV in both the CC and the EC. The resolution is slightly worse in the ICR (16% at  $p_T = 50$  GeV to 11% at  $p_T = 400$  GeV). The method to unfold the data uses a four-parameter ansatz function [11] to parametrize the  $p_T$  dependence of the jet cross section

$$f(N, \alpha, \beta, \gamma) = N \left( \frac{p_T}{\text{GeV}} \right)^{-\alpha} \left( 1 - \frac{2 \cosh(y^{\min}) p_T}{\sqrt{s}} \right)^{\beta} e^{-\gamma p_T}$$

convoluted with the measured jet  $p_T$  resolution. Here  $y^{\min}$  is the lowest edge of the  $|y|$  bin. This ansatz function is convoluted with the measured  $p_T$  resolution and fitted to the experimental data. The correction factor for each bin of the jet cross section is then determined as the ratio of the original ansatz function and the one convoluted with the  $p_T$  resolution. The unfolding corrections vary between 0.8 for a jet  $p_T \sim 50$  GeV and 0.6 at 400 GeV in the CC. In the EC and the ICR, the corrections are  $> 0.8$  at low  $p_T$ , but decrease to 0.2 at the largest  $p_T$  and  $y$ . The  $y$  resolution is better than 0.05 for jets with  $p_T > 50$  GeV and 0.01 at 400 GeV, and leads to an unfolding correction of 0.98–1.00 in most bins, and 0.9 in the highest  $y$  bins. The purity of the most forward  $y$  bins at high  $p_T$  is small (down to 20%) due to the  $p_T$  resolution, but the highest  $p_T$  bins, where the measurement is performed, are chosen so that the statistical significance of the measurement has a 95% confidence level.

The results of the inclusive jet cross section measurement are displayed in Fig. 1 in six  $y$  bins as a function of  $p_T$ . The cross section extends over eight orders of magnitude across the full  $p_T$  range. Perturbative QCD predictions in next-to-leading order (NLO) in  $\alpha_S$ , computed using the fastNLO program [12] (based on NLOJET++ [13]) and the PDFs from CTEQ6.5M [14] and MRST2004 [15], are compared to the data. The renormalization and factorization scales ( $\mu_R$  and  $\mu_F$ ) are set to the individual jet  $p_T$ . Predictions are corrected for non-perturbative contributions due to underlying event and hadronization computed by PYTHIA with the CTEQ6.5M PDFs, the QW tune [16], and the 2-loop formula for  $\alpha_S$ . The PYTHIA cross section is reweighted in partonic center-of-mass energy so that

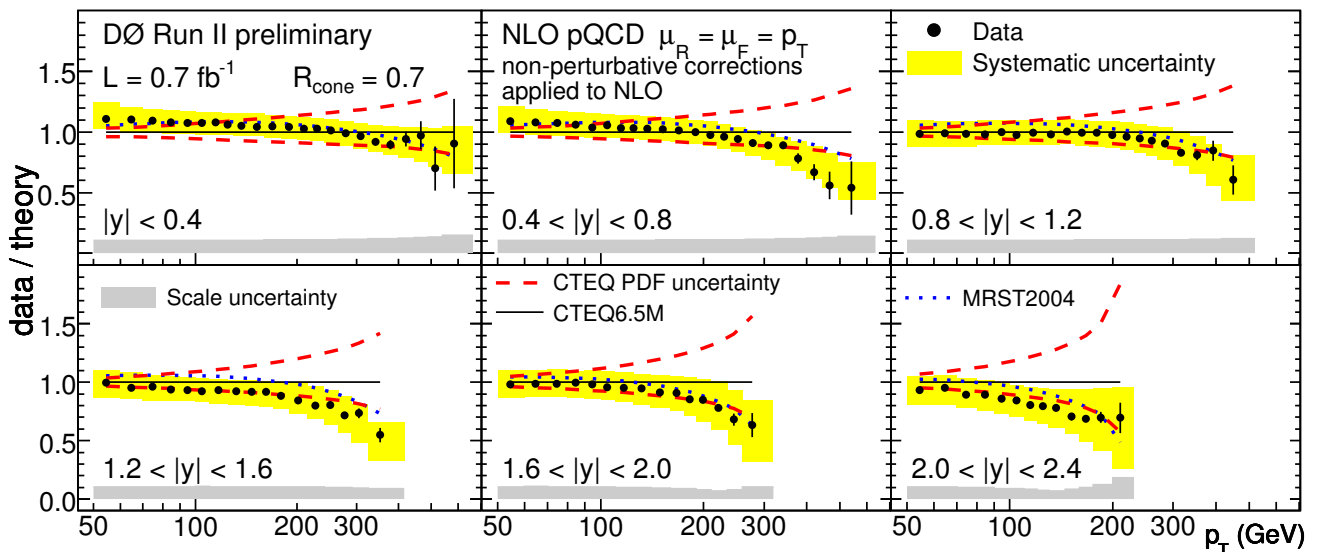


FIG. 2: Measured data divided by theory for the inclusive jet cross section as a function of jet  $p_T$  in six  $y$  bins. The data systematic uncertainties, including 6.1% from the luminosity determination, are displayed as a shaded band. NLO pQCD calculations, with renormalization and factorization scales set to jet  $p_T$  using the CTEQ6.5M PDFs and including non-perturbative corrections, are compared to the data. The CTEQ6.5 PDF uncertainties are shown as dashed lines and the predictions with MRST2004 PDFs as dotted lines. The theoretical uncertainty, determined by changing the renormalization and factorization scales between  $p_T/2$  and  $2p_T$ , is shown at the bottom of each figure.

the PYTHIA parton showers agree with the NLO pQCD calculations. These non-perturbative corrections to theory extend from (+10%) to (+20%) at  $p_T \sim 50$  GeV between  $|y| < 0.4$  and  $2.0 < |y| < 2.4$ . The corrections are of order (+5%) for  $p_T \sim 100$  GeV, and smaller than (+2%) above 200 GeV.

The ratio of the data to the theory is shown in Fig. 2. The dashed lines show the uncertainties on the PDFs coming from the CTEQ6.5 parametrizations. The predictions from MRST2004 [15] are displayed by the dotted line. The predictions agree well with the data except for a tendency for the data to be lower than the central CTEQ prediction — particularly at large  $p_T$  — but mostly within the CTEQ PDF uncertainty band. The  $p_T$  shape of the data is well reproduced by the MRST parametrization. The size of the experimental systematic uncertainty is comparable to the PDF uncertainties. The theoretical scale uncertainty, obtained by varying the factorization and renormalisation scales between  $\mu_R = \mu_F = p_T/2$  and  $\mu_R = \mu_F = 2p_T$  is typically between 10–15%. The experimental uncertainties are of the same order as the theoretical ones; NNLO pQCD calculations are expected to reduce the impact of scale uncertainties on QCD fits [17].

Correlations between systematic uncertainties are studied in detail to increase the impact of these data on global PDF fits. Point-to-point correlations in  $p_T$  and  $y$  are determined for each source of systematic uncertainty. The relative uncertainties on the cross section measurement are shown in Fig. 3 for the five most significant sources of systematic uncertainty in  $|y| < 0.4$  and  $2.0 < |y| < 2.4$ . The global luminosity uncertainty of 6.1%, fully correlated in  $y$  and  $p_T$ , is not displayed in Fig. 3. The other  $y$  bins have similar correlations in shape and values between these two extreme bins. The total uncorrelated uncertainty is  $< 3\%$  in the CC, and  $< 15\%$  in the EC.

The two largest systematic uncertainties are due to the electromagnetic energy scale obtained from  $Z \rightarrow e^+e^-$  events [18], and the photon energy scale in the CC obtained using the difference in the calorimeter response between photons and electrons in the detector simulation. The uncertainty on photon energy scale is mainly due to the knowledge of the amount of dead material in front of the calorimeter and from the physics modeling of electromagnetic showers in the GEANT-based [10] simulation. Both contributions to the jet cross section are  $\approx 5\%$  in the CC and 5 – 15% in the EC.

The large- $p_T$  extrapolation of jet energy scale is determined using the detector simulation with the single-pion response tuned to  $\gamma$ +jet data. The uncertainty rises to 12% (30%) in the CC (EC), and is dominated by the uncertainty in the jet fragmentation, estimated by comparing the fragmentation models in PYTHIA and HERWIG. The uncertainty in  $y$  intercalibration corresponds to systematic uncertainties associated with the procedure to equalize the calorimeter response in different regions of  $y$  in dijet events. The systematic uncertainties are small in the CC, but extend up to 25% in the EC. Finally, systematic uncertainties associated with showering effects, due primarily to the description of the shower within the detector and differences between PYTHIA and HERWIG, range from 3% at low  $p_T$  to 7% (15%) at large  $p_T$  in the CC (EC).

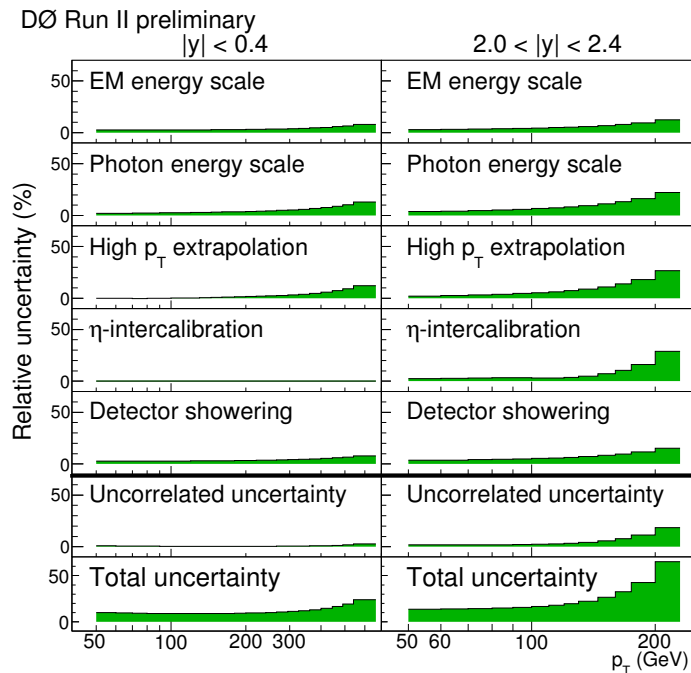


FIG. 3: Effect of point-to-point correlations for  $|y| < 0.4$  and  $2.0 < |y| < 2.4$  as a function of jet  $p_T$ . The largest systematic uncertainties correspond to electromagnetic and photon energy scale, high  $p_T$  extrapolation,  $y$  intercalibration and detector showering effects. The uncorrelated and total systematic uncertainties if information on point-to-point correlations are not available are also displayed to indicate the impact on the total systematic uncertainty. The luminosity uncertainty of 6.1%, fully correlated in  $y$  and  $p_T$ , is not displayed.

To show the potential impact of using point-to-point uncertainty correlations in jet rapidity and transverse momentum on PDF determination, we give in Fig. 3 the uncorrelated and total systematic uncertainties as a function of jet  $p_T$  as a percentage of the jet cross section measurement. The total uncorrelated uncertainties are 25% and 15% of the full uncertainties in the CC and EC respectively. The full systematic uncertainties are similar in size to the PDF uncertainties (Fig. 2) and the performed detailed analysis of the correlations will make it possible to further constrain the PDFs. Knowledge of these correlations is especially important for constraining the PDFs in NNLO pQCD fits [17] where the scale dependent uncertainties are smaller.

In conclusion, the measured inclusive jet cross section in  $p\bar{p}$  collisions at  $\sqrt{s} = 1.96$  TeV with  $\mathcal{L} = 0.7$  fb $^{-1}$  is presented for six  $y$  bins as a function of  $p_T$ , extending the kinematic reach and precision of existing inclusive jet measurements. NLO pQCD calculations with CTEQ6.5M or MRST2004 PDFs agree with the data and favor the lower edge of the CTEQ6.5 PDF uncertainty band at large  $p_T$  for CTEQ6.5 and the shape of the  $p_T$  dependence for MRST2004. A full analysis of correlations between sources of systematic uncertainty is performed, increasing the potential impact of these data on global PDF fits. These data can be used to further constrain the PDFs especially for QCD fits performed at NNLO which is fundamental for precise theory predictions for the LHC physics program and for searches for new phenomena in the jet channel.

- 
- [1] T. Andeen *et al.*, FERMILAB-TM-2365-E (2006).
  - [2] CDF Collaboration, A. Abulencia *et al.*, Phys. Rev. **D75**, 092006 (2007), Phys. Rev. Lett. **96**, 122001 (2006).
  - [3] D0 Collaboration, B. Abbot *et al.*, Phys. Rev. Lett. **82**, 2451 (1999).
  - [4] CDF Collaboration, F. Abe *et al.*, Phys. Rev. Lett. **77**, 438 (1996).
  - [5] A. Belyaev, J. Pumplin, W. K. Tung, and C. P. Yuan, JHEP **0601**, 069 (2006); S. Ferrag, arXiv:hep-ph/0407303.
  - [6] D0 Collaboration, V. M. Abazov *et al.*, Nucl. Instrum. Methods **A565**, 463 (2006).
  - [7] Pseudorapidity is defined as  $\eta = -\log(\tan \frac{\theta}{2})$ , where  $\theta$  is the polar angle relative to the proton beam direction, measured with respect to the detector center.
  - [8] G. C. Blazey *et al.*, in *Proceedings of the Workshop: "QCD and Weak Boson Physics in Run II"*, edited by U. Baur, R. K. Ellis, and D. Zeppenfeld, Batavia, Illinois (2000) p. 47.
  - [9] T. Sjöstrand *et al.*, Comp. Phys. Comm. **135**, 238 (2001).

- [10] CERN Program Library Long Writeup Report No. W5013, 1993; documentation available at <http://wwwasd.web.cern.ch/wwwasd/geant>.
- [11] D0 Collaboration, B. Abbot *et al.*, Phys. Rev. **D64** 032003 (2001).
- [12] T. Kluge *et al.*, arXiv:hep-ph/0609285.
- [13] Z. Nagy, Phys. Rev. Lett. **88**, 122003 (2002); Phys. Rev. **D68**, 094002 (2003).
- [14] W. K. Tung *et al.*, JHEP **0702** 053 (2007); J. Pumplin *et al.*, JHEP **0207**, 12 (2002); D. Stump *et al.*, JHEP **0310**, 046 (2003).
- [15] A. D. Martin *et al.*, Phys. Lett. **B604**, 61 (2004).
- [16] R. Field in: M. G. Albrow *et al.* [TeV4LHC QCD Working Group], arXiv:hep-ph/0610012.
- [17] A. D. Martin *et al.*, Phys. Lett. **B652**, 292 (2007); A. D. Martin *et al.*, Phys. Lett. **B531**, 216 (2002); Eur. Phys. J. **C18**, 117 (2000); N. Kidonakis, J. F. Owens, Phys. Rev. **D63**, 054019 (2001), D. Stump *et al.*, JHEP **0310**, 046 (2003).
- [18] D0 Collaboration, V. M. Abazov *et al.*, Phys. Rev. **D76**, 012003 (2007).
- [19] G. Marchesini *et al.*, Comp. Phys. Comm. **67**, 465 (1992); G. Corcella *et al.*, JHEP **0101**, 010 (2001).